

The effect of the impurities on the magnetic, electronic and optical properties of Mn_5Ge_3



Vyacheslav Zhandun*, Aleksey Matsynin

Kirensky Institute of Physics - Federal Research Center "Krasnoyarsk Science Centre, Siberian Branch of the Russian Academy of Sciences", 660036 Krasnoyarsk, Russia

ARTICLE INFO

Keywords:

Ab initio calculations
Mn-Ge system
 Mn_5Ge_3 alloy
Nowotny $\text{Mn}_5\text{Ge}_3\text{O}_x$ phase
Magnetic properties
Impurities
Spin-crossover

ABSTRACT

Earlier, we experimentally showed a significant effect of oxygen on the magnetic and structural properties of Mn_5Ge_3 due to the formation of a Nowotny phase of $\text{Mn}_5\text{Ge}_3\text{O}_x$. Here, in continuation of this study, we present a theoretical study of the magnetic and electronic properties of Mn_5Ge_3 and $\text{Mn}_5\text{Ge}_3\text{D}_x$ ($D = B, C, O$). It was found that hexagonal Mn_5Ge_3 is a ferromagnetic metal with two nonequivalent manganese atoms in the structure. Our ab initio calculations also predict the existence of a spin-crossover in Mn_5Ge_3 under pressure. Impurities reduce saturation magnetization and electrical and thermal conductivity; however, the magnetic susceptibility and Curie temperature increase. Microscopic mechanisms of the effect of the impurities on the magnetic and electronic properties Mn_5Ge_3 are discussed.

1. Introduction

Recently, the structural, electronic, and magnetic properties of ferromagnetic bulk Mn_5Ge_3 crystals and thin films have been thoroughly studied due to their possible application in the field of spintronics. [1–5]. Mn_5Ge_3 has a number of attractive features, such as a high spin polarization [[6],[7]] and the possibility of epitaxial growth on Ge(111) and Ge(001) substrates [8–11]. These two facts allows the Mn_5Ge_3 compound to be a potential source of spin injection into the Ge [8–11] layer in the epitaxial samples of $\text{Mn}_5\text{Ge}_3/\text{Ge}$ (111) and $\text{Mn}_5\text{Ge}_3/\text{Ge}$ (001).

The present work was inspired by our recent experimental success in solid-state synthesis and characterization of ferromagnetic Mn_5Ge_3 nanoclusters in GeO/Mn thin films [12]. We have shown the considerable effect of oxygen on chemical and physical properties of Mn_5Ge_3 nanoclusters. Chemical properties are associated with a change in the temperature of the onset of solid-phase synthesis of the ferromagnetic phase from 120 to 180 °C. The physical properties of $\text{Mn}_5\text{Ge}_3\text{O}_x$, in particular the magnetic ones, have also changed compared to the pure Mn_5Ge_3 phase; namely, a significant increase in saturation magnetization to 600 emu/ cm^3 , and an increase in the Curie temperature from 300 K to 400 K was obtained. It was suggested that the increase in the Curie temperature and magnetization is due to the migration of C and O impurities to the Mn_5Ge_3 lattice and the formation of the Nowotny phase of $\text{Mn}_5\text{Ge}_3\text{C}_x\text{O}_y$ [13–15]. The possibility of increasing the Curie temperature by doping Mn_5Ge_3 with C and O atoms was also proposed in [[8],[9],[16],[17]]. For example, in $\text{Mn}_5\text{Ge}_3\text{C}_x$ epitaxial films, an increase in the carbon concentration (x) leads to an increase in the Curie temperature, which reaches a maximum $T_C = 460$ K at $x \sim 0.6$ – 0.7 [17]. Other experimental studies have also shown that N, C, and O impurities, which are present even in ultra-high vacuum, migrates into the Mn-Ge nanostructures during precipitation or annealing and change the magnetic and electrical properties [18–21]. However, the microscopic nature of the effect of the impurities

* Corresponding author.

E-mail address: jvc@iph.krasn.ru (V. Zhandun).

<https://doi.org/10.1016/j.cjph.2020.06.027>

Received 9 April 2020; Received in revised form 15 June 2020; Accepted 30 June 2020

Available online 15 September 2020

0577-9073/ © 2020 The Physical Society of the Republic of China (Taiwan). Published by Elsevier B.V. All rights reserved.

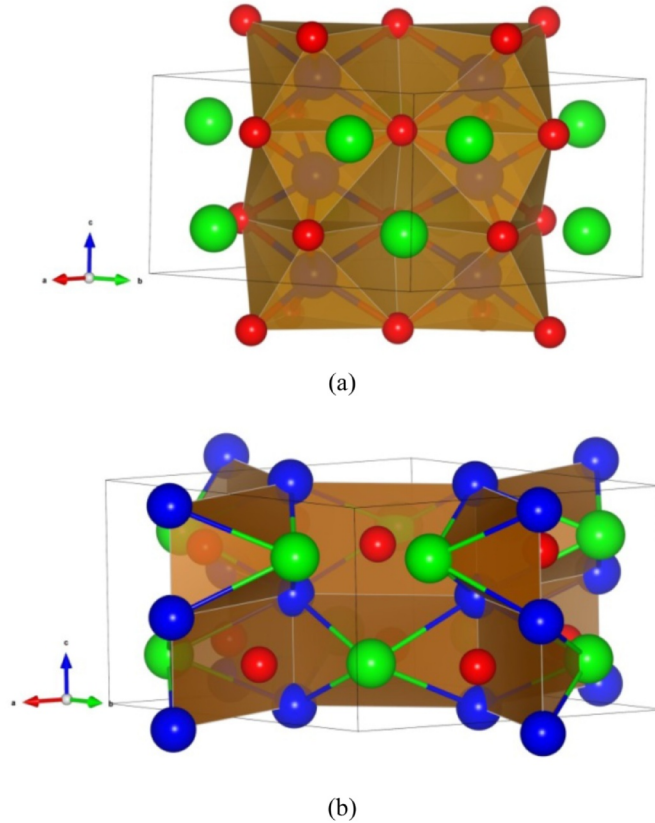


Fig. 1. Crystal structure of Mn_5Ge_3 . (a) Mn-Ge octahedra are highlighted; (b) MnI-MnII tetrahedra are highlighted. MnI, MnII and Ge atoms are shown by green, blue and red balls, correspondingly.

Table. I

The total energies of ferromagnetic (FM), ferrimagnetic (FiM) and nonmagnetic (NM) phases of Mn_5Ge_3 .

Phase	E (eV)
FM	-118.522
FiM	-117.830
NM	-115.492

on the physical properties of Mn with Ge is still poorly understood.

This work is a logical continuation of our experimental work [12] for the theoretical foundation of the observed effects. Herein, we report the results of ab initio calculations of electronic, magnetic, and optical properties of the pure ferromagnetic Mn_5Ge_3 and Mn_5Ge_3 doped by O, C, and B atoms. The paper organized as follows. Section II contains details of calculations. Section IIIa report and discuss the results of calculations of magnetic, electronic, and optical properties of pure Mn_5Ge_3 . In Section IIIb we compare and discuss the results obtained for pure and doped Mn_5Ge_3 , and in the last Section we make conclusions.

2. Calculation details

Ab initio calculations have been performed using the Vienna ab initio simulation package (VASP) [22]. Throughout all calculations, projector augmented wave (PAW) pseudopotentials [23], Perdew-Burke-Ernzerhoff (PBE) parameterization of the exchange-correlation functional [24] and the generalized gradient approximation (GGA) has been used. The valence electron configurations $3d^54s^2$ were taken for Mn atoms and $4s^24p^2$ for Ge atoms. The plane-wave cutoff energy 500 eV is used. The Brillouin-zone integration was performed on the $8 \times 8 \times 8$ Monkhorst-Pack mesh [25].

The temperature dependencies of the electrical conductivity, thermal conductivity, and magnetic susceptibility were calculated using BoltzTrap code [26], i.e., within the semi-classic Boltzmann theory. The obtained in VASP band structures were processed by BoltzTrap code to obtain mentioned above quantities. Since the electrical conductivity and the thermal conductivity are obtained

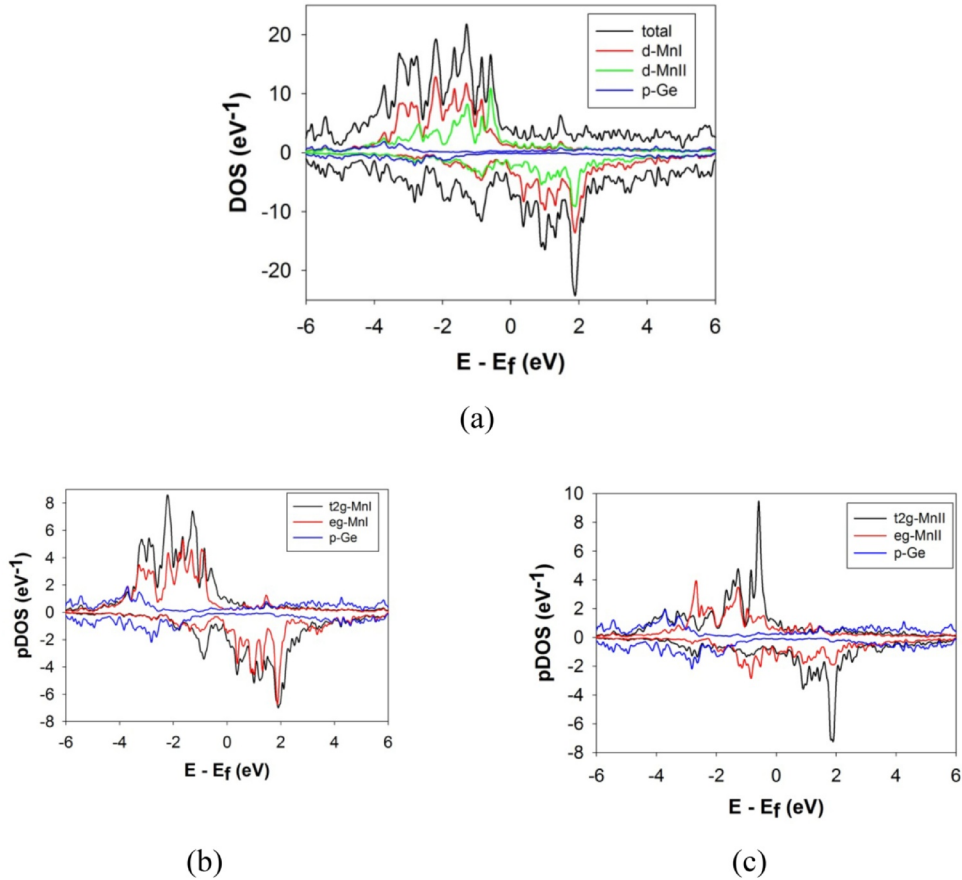


Fig. 2. Total and projected densities of electronic states. Panels (b) and (c) show the contribution of t2g- and eg-orbitals in density of d-states of MnI (b) and MnII (c) atoms. The zero on the energy axis is the Fermi energy. Negative values of DOS correspond to the spin-down states.

within constant relaxation time approximation in BoltzTrap code, the results are given as σ/τ and κ/τ , where τ is relaxation time which needs to be carefully determined.

3. Results and discussion

3.1. The structural, magnetic and electronic properties of the pure Mn_5Ge_3

The manganese germinates Mn_5Ge_3 has a hexagonal crystal structure (space symmetry group $P6_3/mcm$) with two formula units (Fig. 1a). The unit cell contains two nonequivalent manganese atoms: six MnI atoms (Wyckoff position 6g) and four MnII atoms (Wyckoff position 4d). There are four atomic planes in structure along the c-axis can be: the planes at $z = 0$ and $z = 0.5$ are occupied by MnII atoms only, the planes at $z = 1/4$ and $z = 3/4$ are occupied by MnI and Ge atoms. MnII atoms have an octahedral environment: they are surrounded by six germanium ions located at the vertices of the octahedron. MnI atom has three in-plane and two out-of-plane Ge atoms in the local environment.

The geometry of the structure was fully optimized within GGA. Calculated optimized lattice parameters $a = 7.14$ and $c = 4.97$ are close to the experimental lattice parameters [[27,28]], []. We also evaluated the bond lengths between MnII-Ge atoms inside the octahedrons and between MnI-Ge atoms which are: $d_{MnII-O} = 2.52$ Å, $d_{MnI-O} = 2.46$ and 2.6 Å for in-plane neighbors and $d_{MnI-O} = 2.71$ Å for the out-of-plane neighbors. As seen, the distances between the MnII-Ge atoms are on average smaller than ones between MnI-Ge atoms. Magnetic manganese atoms form tetrahedra with MnII atoms at the base and a MnI atom at the top of the tetrahedron (Fig. 1b). The shortest distances between MnI-MnII and MnI-MnII atoms are $d = 3.02$ Å, and the shortest distances between MnII-MnII atoms are $d = 2.48$ Å.

To study the magnetic properties of Mn_5Ge_3 we have compared the energies of three possible phases: nonmagnetic, ferromagnetic and ferrimagnetic. Besides, during the optimization procedure the initial values of magnetic moments on the non-equivalent manganese atoms were taken as equal as well different. As a result we obtained that the ferromagnetic phase is lower in energy (Table 1). The nonequivalent Mn atoms have different magnetic moments: $\mu_{Mn1} = 3.1\mu_B$ and $\mu_{Mn2} = 2.2\mu_B$, i.e., magnetic moments of octahedrally coordinated MnII atoms are smaller than of the Mn1 atoms. The total magnetization is $M_{tot} = 26.8\mu_B$, and it well corresponds with the experimental value: $M_{tot} = 26.8\mu_B$ [[27]]. The total and partial densities of states of Mn_5Ge_3 are shown in Fig. 2. The pure compound is a

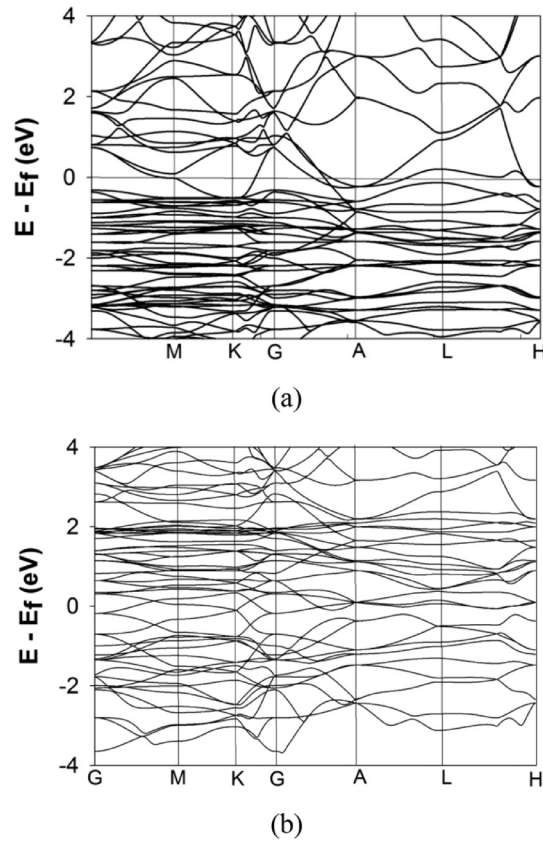


Fig. 3. The majority (a) and minority (b) states band structures of Mn_5Ge_3 . The zero on the energy axis is the Fermi energy.

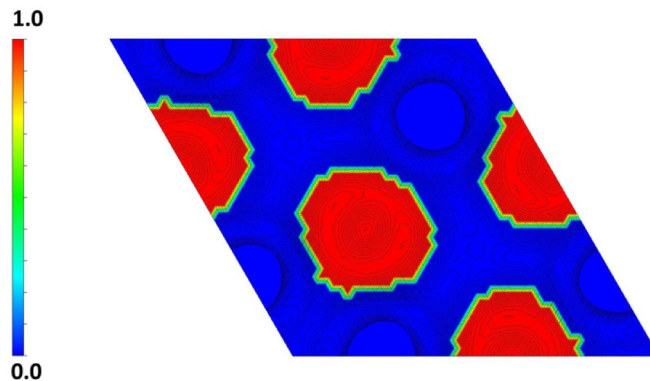


Fig. 4. The electronic localization function. The red color corresponds to the strong localized electrons, blue color to the delocalized electrons.

ferromagnetic metal with the spin polarization $P = -35\%$. The partial density of states of both manganese atoms is located in the approximately same wide energy range indicating strong hybridization between MnI and MnII states. At that, electronic states of MnII are more localized than MnI atom. t_{2g} -states of both manganese atoms are closest to the Fermi energy ($[-4; 0]$ eV) than e_g -states ($[-6; -2]$ eV). P-states of germanium are smeared in the whole energy range. Moreover, if d -states of MnI and Mn II are most hybridized in the energy region near the Fermi energy, then the maximal hybridization of Mn d - and Ge p -states is in the energy range below Fermi energy $[-8; 3]$ eV.

The band structure for the majority and minority spins of Mn_5Ge_3 is shown in Fig. 3a and 3b. One can see that the bands around Fermi energy are rather dispersed for the majority spin states, whereas they are more localized in the minority spin channel. The dispersion around Fermi energy in the majority spin component confirms the strong hybridization between MnI and MnII spin-up d -states, and between Mn and Ge spin-up d - and p -states, correspondingly.

Fig. 4 shows the so-called electron localization function (ELF) [[29]], which displays the degree of localization of electrons in the

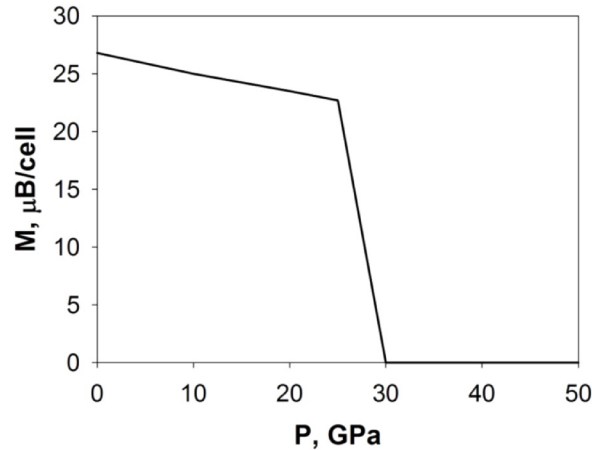


Fig. 5. The pressure dependence of the total magnetization of Mn_5Ge_3 .

cell. This function can lie in the range from 0 to 1, where 0.5 corresponds to the uniform electronic gas and 1 to localized electrons. One can see that electrons are localized near the Ge atoms (red area in Fig. 4) and delocalized in the intermediate space forming electron gas (blue area in Fig. 4). This indicates the predominantly metal character of the bonds in Mn_5Ge_3 .

The intriguing feature of the pure Mn_5Ge_3 is the strong dependence of the total magnetization in Mn_5Ge_3 on the applied hydrostatic pressure. As seen in Fig. 5, at the low-pressure total magnetization smoothly decrease when pressure increase. However, at the pressure above $P = 25$ GPa, the total magnetization abruptly drops to zero, i.e., *ab initio* calculation predict the high-to low-spin crossover at the pressure $P = 25$ GPa. The decrease of magnetization is related to the shift of the spin-up and spin-down density of states of both manganese atoms to each other in the direction of the Fermi energy (Fig. 6). At that, the d -electrons of MnI atom are delocalized stronger than d -electrons of MnII atom.

3.2. The effect of impurities on the electronic, magnetic, and optical properties

As was suggested in [[12],[17]], the migration of oxygen or/and carbon atoms in Mn_5Ge_3 films during film growth and annealing is possible. This leads to the formation of the Nowotny phase $\text{Mn}_5\text{Ge}_3\text{O}_x/\text{Mn}_5\text{Ge}_3\text{C}_x$. This process is accompanied by an increase in magnetization at room temperature and a significant increase in Curie temperature of the obtained compound. At that, the saturation magnetization of $\text{Mn}_5\text{Ge}_3\text{O}_x$ at $T = 0$ K decreases as compared with pure Mn_5Ge_3 . In the present paper, we have studied how the doping of Mn_5Ge_3 by oxygen, carbon atoms, and also boron atoms influence the magnetic and optical properties and electronic structure of the Mn_5Ge_3 compounds. The number and location of doped atoms were varied. Fig. 7 shows two of possible variants of the impurity placement in the structure: the doped atoms can be placed as between neighbor MnII-Ge polyhedral on the MnI-MnII bond (Fig. 7a) as well as on the bond between MnII-MnII atoms (Fig. 7b). The Fig. 8 shows the dependence of the total magnetization on the type and the number of doped atoms. The increase in the number of doped atoms leads to a decrease in the total saturation magnetization as in the experimental measurements. In turn, the behavior of the total magnetization depends on the placement of the impurity in the structure. In the first variant of the impurity placement (Fig. 7a), the doping by oxygen atom has the least apparent effect on the magnetization; the most pronounced decrease of the magnetization occurs for Mn_5Ge_3 doped by boron atoms. In the second variant (Fig. 7b), boron atoms, in contrast, have a smaller effect on the reduction of the magnetization than oxygen and carbon atoms. In both cases, the decrease of the total magnetization due mainly to the reduction in magnetic moment MnII, which falls significantly stronger when doped than the magnetic moment of the MnI atom (see Table II).

The increase of Curie temperature with the doping by O and C atoms observed in [12] can be understood within a simple scenario. In pure Mn_5Ge_3 , the exchange between Mn atoms is direct ($d_{\text{MnII-MnII}} = 2.48 \text{ \AA}$). The doped atoms during annealing can be on the bond between various Mn atoms (see Fig. 8). This leads to the increase in the exchange between magnetic species due to the new shorter superexchange path Mn-X-Mn (X-doped atom) and, as a result, the increase Curie temperature. On the other hand, the placement of an impurity atom between manganese atoms leads to increased delocalization of Mn d -electrons, forming a magnetic moment, on the bonds between them. The consequence of this is a decrease in the magnetic moment of manganese atoms and, as a result of total magnetization of the sample, which is observed experimentally [12] and in the present calculation.

The density of states does not differ significantly when changing the number of doped atoms or when changing the type of dopant (Fig. 9). The main distinction is on the edge of the densities of states. The high-energy empty states are shifted toward the low energy range. At that, spin polarization practically stays the same as for pure Mn_5Ge_3 . Notice that the p -states of the impurities are mainly in the low energy range about $[-10; -15]$ eV.

However, doped atoms adversely affect the temperature dependence of electrical and thermal conductivity. As seen from Fig. 10a,b, the electroconductivity and thermal conductivity fall with the increase of the atomic radius of doped atoms. For example, at room temperature, the electroconductivity decreases almost twice when doped with boron and almost four times when doped with oxygen. However, the magnetic susceptibility of Mn_5Ge_3 slightly increases with the doping (Fig. 10c). At room temperature, the

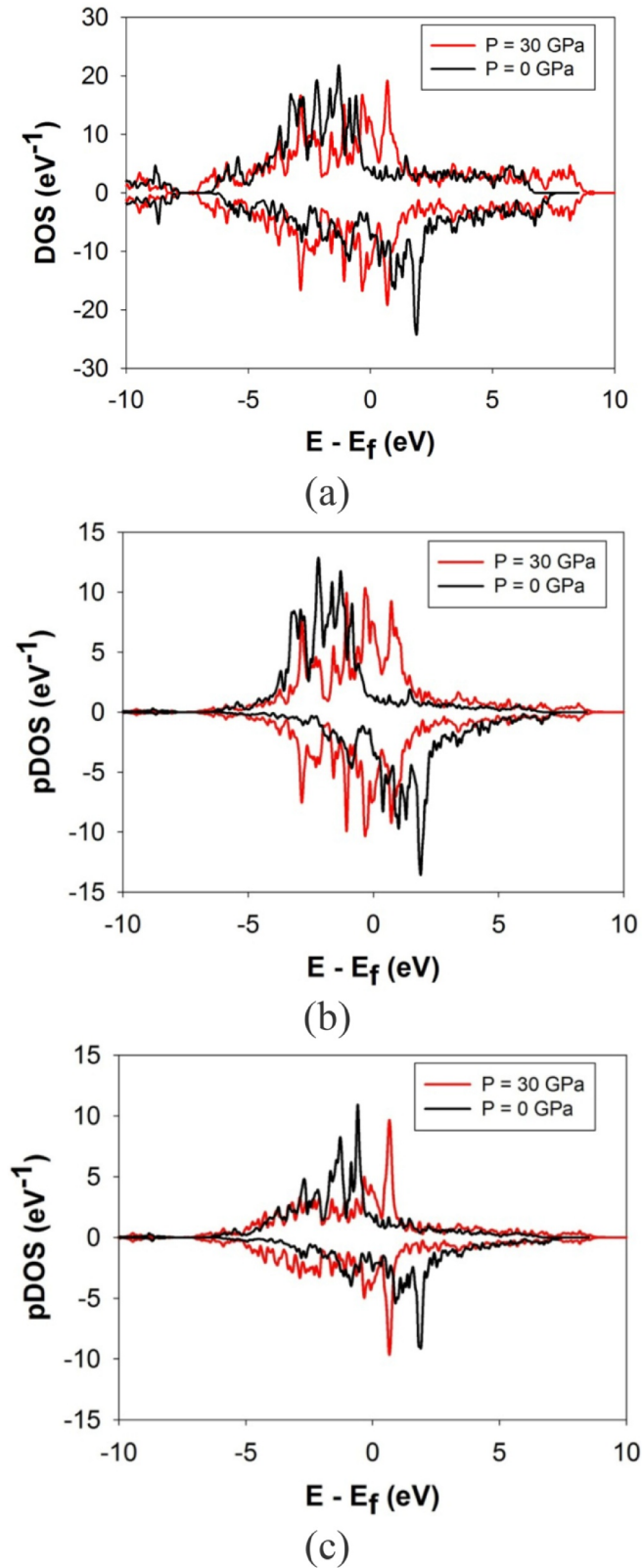


Fig. 6. The comparison of Mn_5Ge_3 densities of states without pressure ($P = 0$ GPa) and under pressure $P = 30$ GPa. Panel (a) shows total density of states, panels (b) and (c) show partial density of d -states of MnI atom (b) and MnII atom(c). The zero on the energy axis is the Fermi energy. Negative values of DOS correspond to the spin-down states.

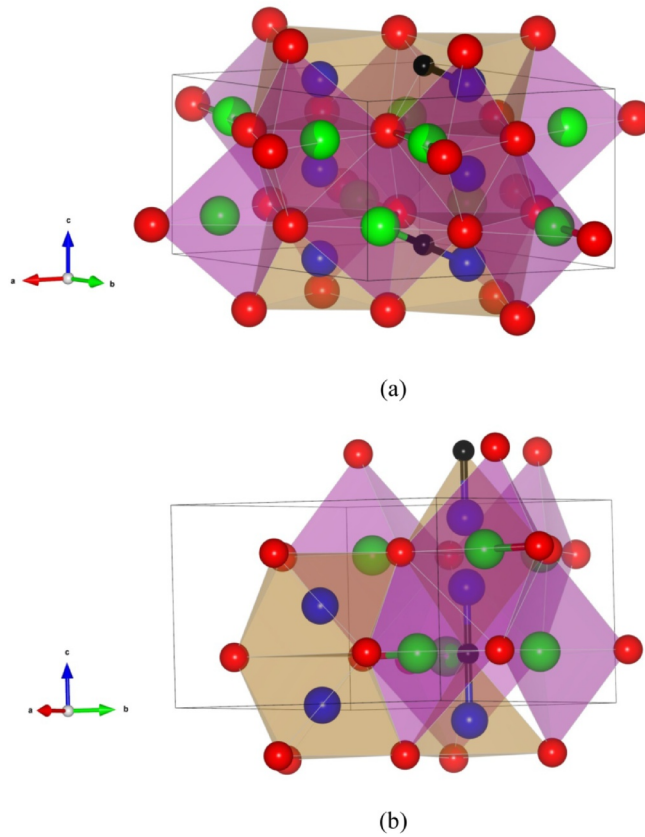


Fig. 7. Two of the possible options for placing impurities on the bonds between manganese atoms. MnI, MnII and Ge atoms are shown by green, blue and red balls, correspondingly. Impurity atom is shown by black ball.

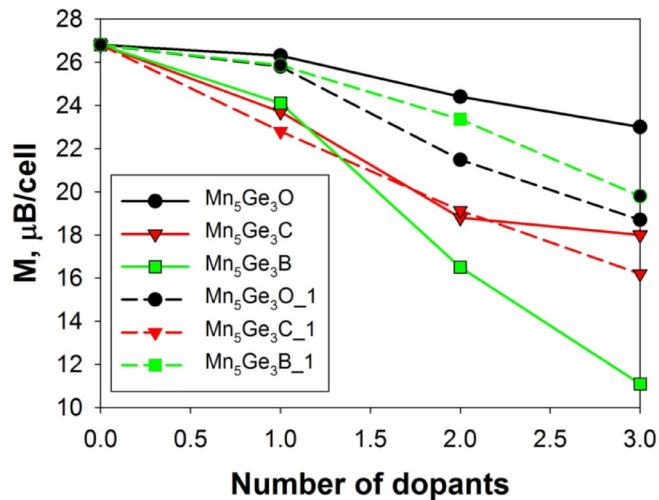


Fig. 8. The dependence of magnetization of the doped Mn₅Ge₃ on the number and type of impurity.

magnetic susceptibility of the Mn₅Ge₃ doped by oxygen exceeds the value for pure compound by 1.2 times. At the same time, at temperatures above 400 K, the maximum value of magnetic susceptibility is observed for the compound doped with boron.

The comparison of the optical properties of the pure and doped Mn₅Ge₃ is shown in Fig. 11. First, we discuss the optical properties of pure Mn₅Ge₃. The imaginary part of the dielectric function (responsible for absorption) drops rapidly in the range [0; 3] eV, one smaller peak is observed in the range [4–7] eV and then ε'' tend to zero. Real part of dielectric function has three poles: at 0.5 eV, 5.3 eV, 13.3 eV. In the range of [5.3; 13.3] eV, the real part of dielectric function is negative, and the absorption spectra have a large

Table. II

The list of MnI and MnII magnetic moments (μ) for the doped Mn_5Ge_3 (the case shown in Fig. 6b).

y	$Mn_5Ge_3B_y$		$Mn_5Ge_3C_y$		$Mn_5Ge_3O_y$	
	μ_{MnI} (μ_B)	μ_{MnII} (μ_B)	μ_{MnI} (μ_B)	μ_{MnII} (μ_B)	μ_{MnI} (μ_B)	μ_{MnII} (μ_B)
1	3.1	1.9	3.1	1.8	3.1	1.9
2	2.9	1.6	2.9	1.5	2.8	1.7
3	2.6	0.5	2.7	0.7	2.7	0.8

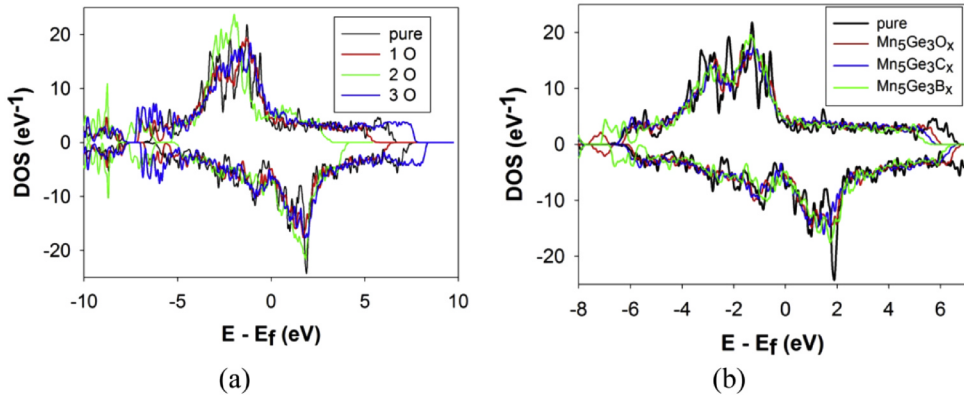


Fig. 9. The comparison of the dependence of the total densities of electronic states of pure and doped Mn_5Ge_3 ; on the number of doped atoms (a); on the type of doped atoms (b). The zero on the energy axis is the Fermi energy. Negative values of DOS correspond to the spin-down states.

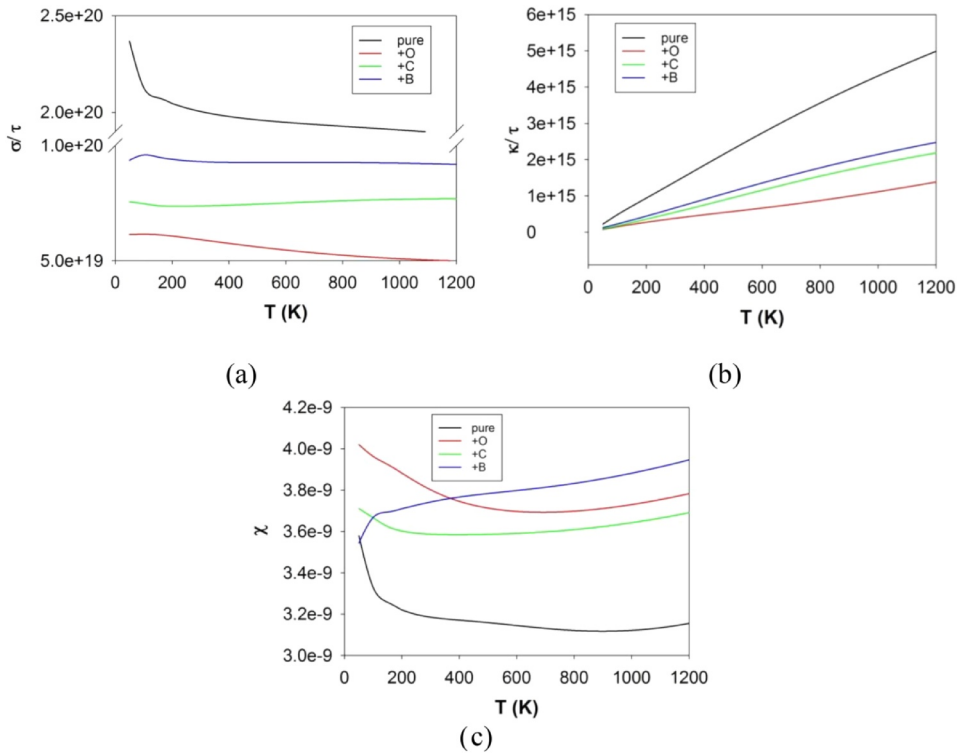


Fig. 10. The temperature dependence of the electroconductivity (a), thermal conductivity (b) and magnetic susceptibility (c).

smearred peak. At 2.4 eV, the ϵ' comes very close to the zero value but does not reach it. Reflectivity drops sharply in the low-energy range, then in the middle range, it begins to rise to $R = 0.7$ at $\omega \sim 10$ eV, and then drops above zero to $\omega = 13.3$ eV. When doping, the behavior and shape of the optical spectra remain qualitatively unchanged; only quantitative changes are observed. So, in doped Mn_5Ge_3 , the absorption band slightly shifts toward the low energy range and becomes narrower with the increase valence number of

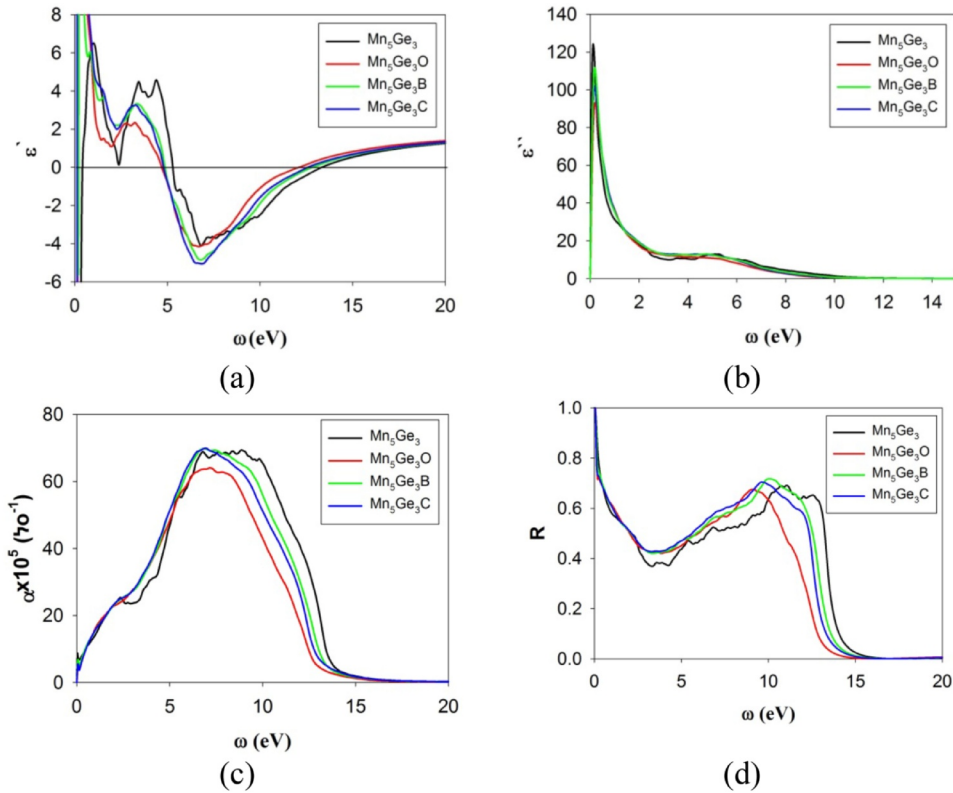


Fig. 11. Optical properties of doped Mn_5Ge_3 : real and imaginary part of dielectric function ((a) and (b)); absorption (c) and reflection spectra (d).

the doping impurity. The similar behavior is observed for the reflectance spectra also. At that, the poles of the real part of dielectric function are also shifted to the low-energy range.

4. Conclusion

We have performed a theoretical study of the effect of the doping by O, C, and B atoms on the magnetic, electronic, and optical properties of Mn_5Ge_3 within the ab initio DFT approach. The magnetic, electronic, and optical properties are calculated. The pure Mn_5Ge_3 was characterized as ferromagnetic metal containing two nonequivalent manganese atoms in accordance with experimental results. The spin-crossover at the hydrostatic pressure in pure Mn_5Ge_3 is predicted. In doped compounds, the change in the electronic structure is not very pronounced, however total magnetization is strongly dependent on the type and number of impurities. The decrease of saturation magnetization at $T = 0$ K and increase of the Curie temperature can be understood in the terms of the forming of the new superexchange path between manganese atoms under doping and the delocalization of Mn d -electrons on these bonds. Electrical conductivity and thermal conductivity decrease in a doped compound compared to pure Mn_5Ge_3 , in contrast to the magnetic susceptibility, which increases in a doped compound. The experimental results of [12] are in well agreement with the theoretical calculations of the present paper.

Declaration of Competing Interest

None.

Acknowledgments

The reported study was funded by Russian Foundation for Basic Research, Government of Krasnoyarsk Territory, Krasnoyarsk Regional Fund of Science to the research projects № № 19-42-240016: « Control of structural, magnetic, electronic, and optical properties by pressure and intercalation into functional compounds with a spinel structure containing 3d and 4f ions» and 18-42-243009: «New magnetic film nanocomposites based on layered GeO/Mn systems: synthesis, experimental and theoretical study of structural and magnetic properties». The calculations were performed with the computer resources of "Complex modeling and data processing research installations of mega-class" SRC "Kurchatovsky Institute" (<http://ckp.urcki.ru>).

References

- [1] R. Kalvig, E. Jedryka, P. Aleshkevych, M. Wojcik, W. Bednarski, M. Petit, L. Michez, Ferromagnetic resonance in Mn_5Ge_3 epitaxial films with weak stripe domain structure, *J. Phys. D Appl. Phys.* 50 (2017) 125001-1–125001-9.
- [2] E. Assaf, A. Portavoce, K. Hoummada, M. Bertoglio, S. Bertaina, High Curie temperature Mn_5Ge_3 thin films produced by non-diffusive reaction, *Appl. Phys. Lett.* 110 (2017) 072408-1 - 072408-4.
- [3] T. Toliński, K. Synoradzki, Specific heat and magnetocaloric effect of the Mn_5Ge_3 ferromagnet, *Intermetallics* 47 (2014) 1–5.
- [4] Y.K. Wakabayashi, R. Akiyama, Y. Takeda, M. Horio, G. Shibata, S. Sakamoto, Y. Ban, Y. Saitoh, H. Yamagami, A. Fujimori, M. Tanaka, S. Ohya, Origin of the large positive magnetoresistance of $\text{Ge}_{1-x}\text{Mn}_x$ granular thin films, *Phys. Rev. B* 95 (2017) 014417-1 - 014417-6.
- [5] C. Sürgers, G. Fischer, P. Winkel, H.v. Löhneysen, Magnetotransport in ferromagnetic Mn_5Ge_3 , $\text{Mn}_5\text{Ge}_3\text{C}_{0.8}$ and $\text{Mn}_5\text{Si}_3\text{C}_{0.8}$ thin films, *Phys. Rev. B* 90 (2014) 104421-1–104421-9.
- [6] R.P. Panguluri, C. Zeng, H.H. Weitering, J.M. Sullivan, S.C. Erwin, B. Nadgorny, Spin polarization and electronic structure of ferromagnetic Mn_5Ge_3 epilayers, *Phys. Status Solidi (b)* 242 (2005) R67–R69.
- [7] Yu.S. Dedkov, M. Holder, G. Mayer, M. Fonin, A.B. Preobrajenski, Spin-resolved photoemission of a ferromagnetic $\text{Mn}_5\text{Ge}_3(001)$ epilayer on $\text{Ge}(111)$, *J. Appl. Phys.* 105 (2009) 073909-1 - 073909-4.
- [8] V.L. Thanh, A. Spiesser, M.-T. Dau, S.F. Olive-Mendez, L.A. Michez, M. Petit, Epitaxial growth and magnetic properties of $\text{Mn}_5\text{Ge}_3/\text{Ge}$ and $\text{Mn}_5\text{Ge}_3\text{C}_x/\text{Ge}$ heterostructures for spintronic applications, *Adv. Nat. Sci. Nanosci. Nanotechnol.* 4 (2013) 043002-1–043002-9.
- [9] M. Petit, L. Michez, C.-E. Dutoit, S. Bertaina, V.O. Dolocan, V. Heresanu, M. Stoffel, V.L. Thanh, Very low-temperature epitaxial growth of Mn_5Ge_3 and $\text{Mn}_5\text{Ge}_3\text{C}_{0.2}$ films on $\text{Ge}(111)$ using molecular beam epitaxy, *Thin Solid Films* 589 (2015) 427–432.
- [10] A. Alvidrez-Lechuga, R. López Antón, J. Trinidad Holguín-Momaca, F. Espinosa-Magaña, S. Federico Olive-Méndez, Role of the substrate temperature on the growth of Mn_5Ge_3 thin films by co-deposition of Mn and Ge on $\text{Ge}(001)$ substrates by magnetron sputtering, *Thin Solid Films* 616 (2016) 111–115.
- [11] S. Yada, P.N. Hai, S. Sugahara, M. Tanaka, Structural and magnetic properties of $\text{Ge}_{1-x}\text{Mn}_x$ thin films grown on $\text{Ge}(001)$ substrates, *J. Appl. Phys.* 110 (2011) 073903-1–073903-8.
- [12] V.G. Myagkov, A.A. Matsynin, L.E. Bykova, V.S. Zhigalov, M. Yu.L., M.N. Volochayev, D.A. Velikanov, A.S. Aleksandrovsky, G.N. Bondarenko, Solid-state synthesis and characterization of ferromagnetic Mn_5Ge_3 nanoclusters in GeO/Mn thin films, *J. Alloys Compd.* 782 (2019) 632–640.
- [13] V.G. Myagkov, V.S. Zhigalov, A.A. Matsynin, L.E. Bykova, Y.L. Mikhlin, G.N. Bondarenko, G.S. Patrin, G.Yu. Yurkin, Formation of ferromagnetic germanides by solid-state reactions in $20\text{Ge}/80\text{Mn}$ films, *Thin Solid Films* 552 (2014) 86–91.
- [14] V.G. Myagkov, V.S. Zhigalov, A.A. Matsynin, L.E. Bykova, G.V. Bondarenko, G.N. Bondarenko, G.S. Patrin, D.A. Velikanov, Phase transformations in the Mn-Ge system and in $\text{Ge}_x\text{Mn}_{1-x}$ diluted semiconductors, *JETP Lett.* 96 (2012) 40–43.
- [15] V.G. Myagkov, L.E. Bykova, A.A. Matsynin, M.N. Volochaev, V.S. Zhigalov, I.A. Tamasov, Yu.L. Mikhlin, D.A. Velikanov, G.N. Bondarenko, Solid state synthesis of Mn_5Ge_3 in $\text{Ge}/\text{Ag}/\text{Mn}$ trilayers: structural and magnetic studies, *J. Solid State Chem.* 246 (2017) 379–387.
- [16] M. Gajdzik, C. Sürgers, M.T. Kelemen, H.V. Löhneysen, Strongly enhanced Curie temperature in carbon-doped Mn_5Ge_3 films, *J. Magn. Magn. Mater.* 221 (2000) 248–254.
- [17] A. Spiesser, I. Slipukhina, M.-T. Dau, E. Arras, V. Le Thanh, L. Michez, P. Pochet, H. Saito, S. Yuasa, M. Jamet, J. Derrien, Control of magnetic properties of epitaxial $\text{Mn}_5\text{Ge}_3\text{C}_x$ films induced by carbon doping, *Phys. Rev. B* 84 (2011) 165203-1–165203-7.
- [18] W. Yin, C.D. Kell, L. He, M.C. Dolph, C. Duska, J. Lu, R. Hull, J.A. Floro, S.A. Wolf, Enhanced magnetic and electrical properties in amorphous Ge: Mn thin films by non-magnetic cooping, *J. Appl. Phys.* (2012) 111.
- [19] S. Tardif, S. Cherifi, M. Jamet, T. Devillers, A. Barski, D. Schmitz, N. Darowski, P. Thakur, J.C. Cezar, N.B. Brookes, R. Mattana, J. Cibert, Exchange bias in GeMn nanocolumns: the role of surface oxidation, *Appl. Phys. Lett.* (2010) 97.
- [20] B. Toydemir, A.C. Onel, M. Ertas, L. Colakerol Arslan, Role of nitrogen on the magnetic properties of MBE grown $\text{Mn}_{0.04}\text{Ge}_{0.96}$ films, *J. Magn. Magn. Mater.* 393 (2015) 220–225.
- [21] P. De Padova, J.-P. Ayoub, I. Berbezier, J.-M. Mariot, A. Taleb-Ibrahimi, M.C. Richter, O. Heckmann, A.M. Testa, D. Fiorani, B. Olivieri, S. Picozzi, K. Hricovini, $\text{Mn}_x\text{Ge}_{1-x}$ thin layers studied by TEM, X-ray absorption spectroscopy and SQUID magnetometry, *Surf. Sci.* 601 (2007) 2628–2631.
- [22] G. Kresse, J. Furthmüller, Efficient iterative schemes for ab initio total-energy calculations using a plane-wave basis set, *Phys. Rev. B* 54 (1996) 11169.
- [23] P.E. Blochl, Projector augmented-wave method, *Phys. Rev. B* 50 (1994) 17953.
- [24] J.P. Perdew, K. Burke, M. Ernzerhof, Generalized gradient approximation made simple, *Phys. Rev. Lett.* 77 (1996) 3865.
- [25] H.J. Monkhorst, J.D. Pack, Special points for Brillouin-zone integrations, *Phys. Rev. B* 13 (1976) 5188.
- [26] G.K.H. Madsen, D.J. Singh, BoltzTraP. A code for calculating band-structure dependent quantities, *Comput. Phys. Commun.* 67 (2006) 175.
- [27] R. Ciszewski, Magnetic Structure of the Mn_5Ge_3 Alloy, *Phys. Status Solidi B* 3 (1963) 1999–2004.
- [28] C. Zeng, S.C. Erwin, L.C. Feldman, A.P. Li, R. Jin, Y. Song, J.R. Thompson, H.H. Weitering, Magnetic and electrical transport properties of $\text{Ge}_{1-x}\text{Mn}_x$ thin films, *Appl. Phys. Lett.* 83 (2003) 5002.
- [29] A.D. Becke, K.E. Edgecombe, A simple measure of electron localization in atomic and molecular systems, *J. Chem. Phys.* 92 (1990) 5397.